

Experimental study of masonry infill reinforced concrete frames with and without corner openings

Hamid Reza Khoshnoud^{*1} and Kadir Marsono^{2a}

¹Department of Civil Engineering, Islamic Azad University, Langroud Branch, Langroud, Iran

²Faculty of Civil Engineering, University of Technology of Malaysia, Skudai, Johor, Malaysia

(Received April 3, 2015, Revised December 3, 2015, Accepted January 11, 2016)

Abstract. Reinforced concrete frame buildings with masonry infill walls are one of the most popular structural systems in the world. In most cases, the effects of masonry infill walls are not considered in structural models. The results of earthquakes show that infill walls have a significant effect on the seismic response of buildings. In some cases, the buildings collapsed as a result of the formation of a soft story. This study developed a simple method, called corner opening, by replacing the corner of infill walls with a very flexible material to enhance the structural behavior of walls. To evaluate the proposed method a series of experiments were conducted on masonry infill wall and reinforced concrete frames with and without corner openings. Two 1:4 scale masonry infill walls with and without corner openings were tested under diagonal tension or shear strength and two RC frames with full infill walls and with corner opening infill walls were tested under monotonic horizontal loading up to a drift level of 2.5%. The experimental results revealed that the proposed method reduced the strength of infill wall specimens but considerably enhanced the ductility of infill wall specimens in the diagonal tension test. Moreover, the corner opening in infill walls prevented the slid shear failure of the infill wall in RC frames with infill walls.

Keywords: masonry infill wall; corner opening; reinforcement concrete frames; monotonic lateral load; experimental methods; earthquake engineering

1. Introduction

Reinforced concrete frame buildings with masonry infill walls are one of the most popular structural systems in the world. In most cases, masonry infill walls interact with reinforced concrete frame but generally, these effects are not considered in structural models. Infill walls significantly increase the lateral stiffness of a structure in an elastic state and play a vital role in resistance against earthquakes.

Past experimental results have shown high initial lateral stiffness and low ductility behavior for infill wall. A state of the art report on the testing and modeling of masonry infilled frame was published by Crisafulli (Crisafulliet al. 2000). The seismic response of reinforced concrete frame with infill walls is a key factor studied by researchers (Pujol and Fick 2010). The effects of

*Corresponding author, Assistant Professor, E-mail: hrkhoshnoud@yahoo.com

^aAssociate Professor, E-mail: Akadir@utm.my

openings in the seismic response of RC frames with infill walls is another important issue (Kakaletsis 2009, Tasnimi and Mohebkah 2011). Infill wall made with standard bricks and locked bricks that do not require mortar were investigated by Misira (2012).

The failure modes for infill walls can be categorized as corner crushing, diagonal compression, sliding shear, frame failure, and diagonal cracking (Asteriset *al.* 2011). The infill walls in reinforced frames provide an equal compression diagonal strut that increases the stiffness of the infilled frame by its truss action. Consequently, the presence of infill walls will change the moment resistance frame action to truss action (Murty and Jain 2000), which will increase axial forces and decrease flexural forces in the frame members. The increase of overall stiffness and strength of RC frames is one advantage of infill walls if they are spread uniformly throughout a building and do not impose irregularities (Dolsek and Fajfar 2001). If the infill walls reach ultimate strength, especially in the lower floors of a building, then a soft story collapse may occur, which is a common failure scenario for RC frames with infill walls.

Polyakov (1960) studied laterally loaded infill wall frame systems and found that a gap was formed in non-loaded diagonal wall and full contact occurred in two loaded diagonal ends. He was the first to suggest using an equivalent compression strut. An equivalent strut can substitute for an infill wall in a macro model if it has the same thickness as the infill wall and the same material properties. Based on Polyakov's calculation, which was used in FEMA356 (2000), the relative infill to frame stiffness is as follows

$$\lambda_l h_{col} = \left[\frac{E_{inf} t_{inf} \sin(2\theta)}{4E_{frm} I_{col} h_{inf}} \right]^{\frac{1}{4}} h_{col} \quad (1)$$

Mainstone (1971) used the above equation to find the relative infill to frame flexibility and proposed an equation for the width of equivalent strut as follows

$$a = 0.638 [\lambda_l h_{col}]^{0.4} r_{inf} \quad (2)$$

Therefore, the stiffness of infill wall frame system is

$$K_{inf} = \frac{A_{strut} E_{inf}}{r_{inf}} \cos^2(\theta) \quad (3)$$

In the above equations, E_{inf} and E_{frm} are the elasticity modulus for the infill and frame, h_{inf} and t_{inf} are the height and thickness of the infill wall, h_{col} , I_{col} , and θ are the height, moment of inertia, and angle of diagonal for the infill with horizon. λ_l is the coefficient used to determine the equivalent width for an infill strut. A_{strut} is the cross sectional area of the equivalent strut and r_{inf} is the diagonal length of the infill (Fig. 1). Holmes (1961) (Eq. (4)), Liauw and Kwan (1984) (Eq. (5)) and Paulay and Priestley (1992) (Eq. (6)) proposed the following equation to estimate the width of an equivalent strut

$$a = \frac{r_{inf}}{3} \quad (4)$$

$$a = \frac{0.95 h_{inf} \cos \theta}{\sqrt{\lambda_l h_{col}}} \quad (5)$$

$$a = \frac{r_{inf}}{4} \tag{6}$$

Eqs. (1) to (3) were used in this study to calculate the relative infill to frame stiffness, the width of equivalent strut, and the stiffness of the infill wall, respectively. The lateral stiffness of a one span one story bare frame with realistic flexural beam stiffness can be calculated by matrix structural analysis as follows

$$K = \frac{24EI_c}{h^3} \left[\frac{L + 6h}{4L + 6h} \right] \tag{7}$$

In Eq. (7), E is the modulus of elasticity for frame members, I_c , I_b , h ($h=h_{col}$) and L is the moment of inertia for the columns and beam, height of the columns, and length of the beam, respectively.

One of the primary objectives of this study was to consider the effects of corner openings in infill walls on the stiffness, strength, and ductility of infill walls and RC frames. Corner openings in this paper means making an opening in the corner of infill wall in each panel and filling the opening with a very soft and high flexible material such as Polystyrene. To achieve this goal, tests are conducted. A diagonal shear strength test was conducted using two 1:4 scale infill wall specimens with and without corner opening. The effect of a monotonically lateral load was conducted using two 1:4 scale RC frames with infill walls with and without corner openings. The results for various stiffness, strength, and energy dissipation related parameters were compared.

2. Experimental study

The experimental study included two series of tests. The first series included two 1:4 scaled

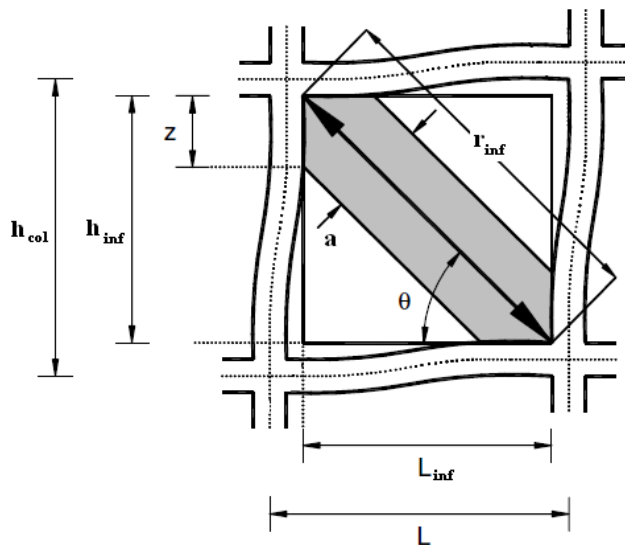


Fig. 1 Masonry infilled frame

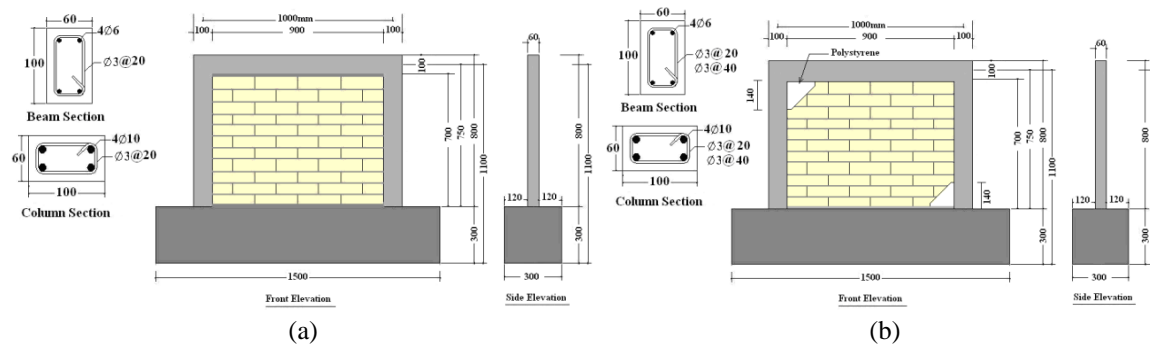


Fig. 2 Schematic view of (a) F1 (b) F2 specimens

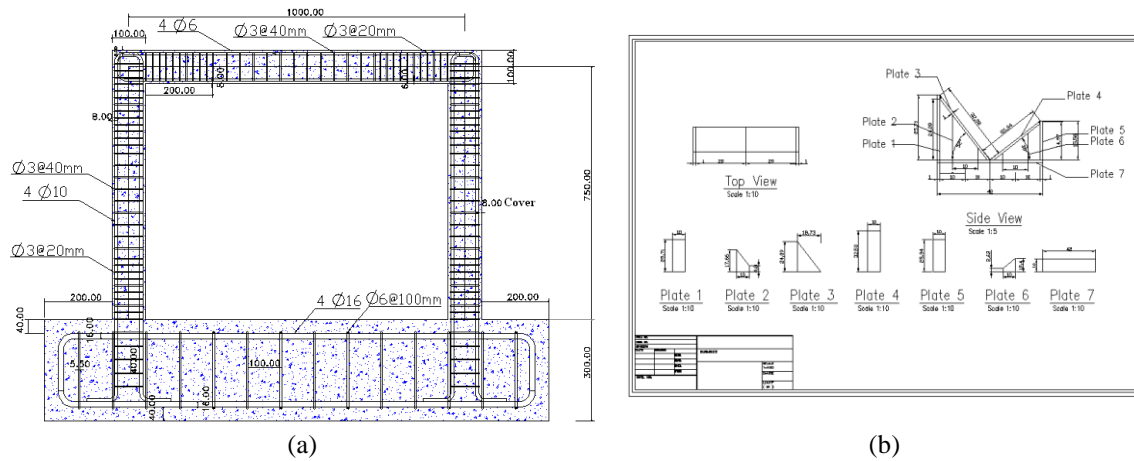


Fig. 3 (a) Reinforcement details for frames (b) Details of loading shoes

wall specimens with and without corner openings for diagonal shear tests, which were called W1 and W2, respectively. In the second series, two one bay one story 1:4 scaled reinforced concrete (RC) frame specimens were used. The first full infill wall (F1) and the second full infill frame with corner openings (F2) were subjected to a lateral load. The frames were 1000 mm long and 750 mm high. The beams and columns were 100×60 mm (Fig. 2). It was assumed that all the frames were located in a high-level seismic zone with design spectra of 0.3 g. The soil profile was Type III (shear wave velocity 180-360 m/s, $T_0=0.15$, $T_s=0.7$ sec, $S=1.75$) equal to NEHRP (FEMA368, 2000) site class *D*. All frames had intermediate reinforced concrete (RC) moment resistant frame (MRF) systems with behavior factor, $R=7$, and an importance factor of $I=1.0$. The cracked moment of inertia was set at 0.35 I_g for beams and 0.7 I_g for the columns to calculate the design drift for initial analysis and to design the models. The bare frame was designed and analyzed using the Iranian seismic code (CODE2800) and ACI-318-2005. The ductility details for confinement bars were used (Fig. 3(a)).

The diagonal tension test conducted based on ASTM E519, using W1 and W2. The specimens were 0.9×0.7 m. This is the exact size of the infill walls in the RC frames of F1 and F2, instead of the 1.2×1.2 m suggested by ASTM. Based on the dimensions (0.9×0.7 m) of the specimens, the appropriate loading shoes for this test were calculated and constructed (Fig. 3(b)). The thickness of

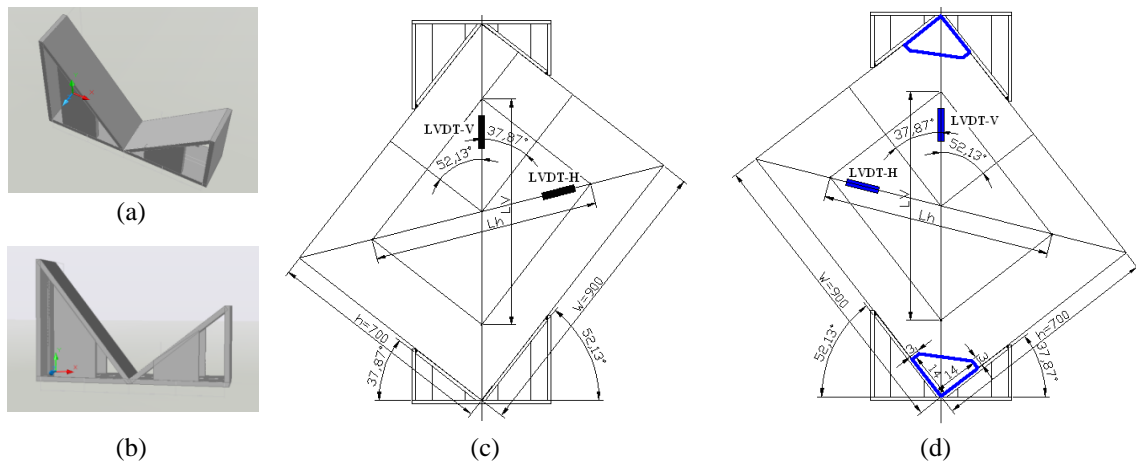


Fig. 4 (a), (b) 3D views of loading shoes, (c) W1 (d) W2 for diagonal shear strength tests

the plates for the loading shoes was 10 mm and the width of the bearings for the shoes was 100 mm. In comparison to the 50 mm thick walls, the dimensions for the loading shoes and bearings for the shoes were large enough to support test walls W1 and W2. The angle of the two sides of the bearing of the shoe was calculated with the rectangular specimen placed in the machine so that its diagonal is in the vertical position and directly under the applied load. Fig. 4(a) and 4(b) provide three-dimensional views of the manufactured loading shoes. Fig. 4(c) and 4(d) show the dimensions of the specimens and location of the linear variable displacement transducer (LVDT) in two main diagonal of walls of W1 and W2. Using the appropriate size of bricks was important because of the scale of models. Small brick produced by the factory had little strength and were more burnt than the full-scale bricks because the size of the small bricks effected the firing process (Egermann 1991). Therefore, in this study, the cutting method suggested by other researchers (Hughes 2000, Taunton 1997), was employed. A clay brick with an approximate size of $215 \times 102.3 \times 65$ mm was used to represent a full sized brick. The clay brick was cut to 8 small pieces with the approximate size of $102.5 \times 53.75 \times 32.5$ mm.

2.1 Material specifications

All models had a 1:4 scale. The maximum size of the aggregates in the concrete was a function of the maximum spacing of the bars and spacing between the main bars and the mold. This spacing decreased when the confinement bars were relocated due to the installation of strain gauges or condensation of sectional bars in the plastic zone of the members. Based on these points and the actual measurements of the spaces in the models, the maximum aggregate size was required to be less than 7 mm. The workability of concrete also played a significant role in casting the concrete in the scaled models. Thus, a super plasticizer was added to the concrete mixtures to increase the workability of the concrete. To control the amount of fine aggregate in the concrete mixture, a sieve analysis was conducted based on ASTM C33/C33M 11a. The specified compressive strength of the cylindrical specimens for the models was about 24 MPa to represent the general concrete used for residential and commercial buildings. Several different trial mixtures were made and tested. In all the trial mixtures, the ratio of water to cement was kept at 0.5 and the workability was

Table 1 The value of materials and admixture in mixture design

Total weight (kg)	Sand (kg)	Cement (kg)	Water (kg)	Plasticizer (ml)
2350	1570	520	260	6240
10	6.681	2.213	1.106	27

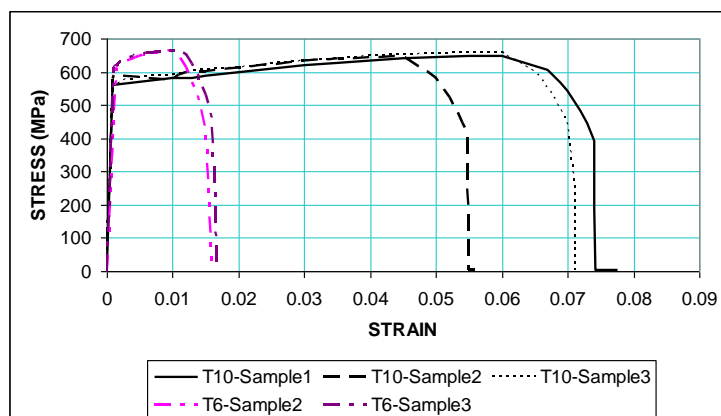


Fig. 5 Stress-strain curve for different samples of bars

increased by adding more super plasticizer. Table 1 shows the final values of sand, cement, water, and super plasticizer for the concrete mixture used for all models. The tensile strength tests for reinforcement concrete bars were performed based on ASTM A615 /A370. Fig. 5 shows the stress-strain curves for bar samples with diameters of 10 mm and 6 mm.

3. Setup of diagonal tension strength test

In this section, the test setup used to test the diagonal tension strength of walls W1 and W2 is presented. Fig. 6(a) shows the loading shoes and base plates of the bottom loading shoes. To avoid any deformation in middle of bottom plate of loading shoe during the test, two thick base plates were added to the bottom loading shoe and one rigid beam was added to the top loading shoe (Fig. 6(b)). The rigid beam uniformly distributed the applied load from the jack to the top loading shoe and increased the stiffness of the top loading shoe against any rotation and deformation. All specimens are constructed in a plywood frame so that the bricks could be leveled, the specimens could be mobilized, and for other test purposes. Fig. 6(c) shows the test specimens with their plywood frame. Fig. 7 shows the setup of diagonal tension strength for W1 and W2.

3.1 Setup of RC frame F1 and F2

The schematics for RC frame model F1 and F2 are shown in Fig. 8. There are two LVDTs (LVDT1 and LVDT2) installed diagonally to measure the shortening and extension of the diagonal compressive and tension of the infill wall. Another pair of LVDTs (LVDT3 and LVDT4) measured the lateral displacement of the frame, one LVDT (LVDT5) measured vertical movement on the mid span of the beam, and LVDT (LVDT6) recorded the rotation of the foundation.

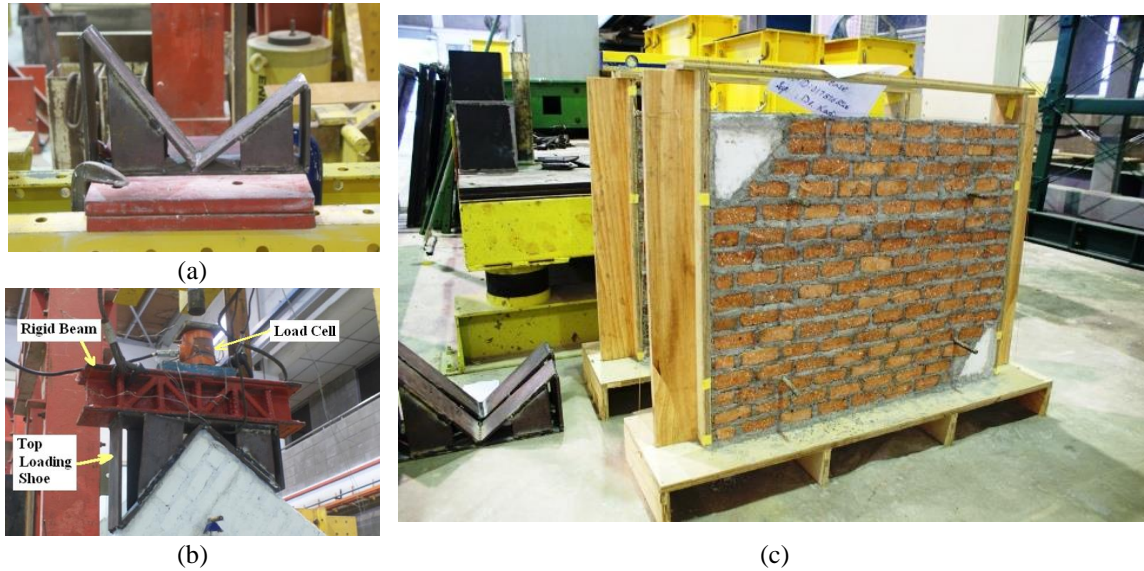


Fig. 6 (a) bottom and (b) top loading shoe details (c) Construction of W1 and W2 specimens



Fig. 7 Setup of (a) W1 and (b) W2 specimens for diagonal shear strength test

In this study, polystyrene was selected to fill corner openings because of its high flexibility, low stiffness, and availability. Polystyrene is a hard plastic but it has more flexibility than the RC frame and masonry infill wall. Polystyrene is a vinyl polymer. Structurally it is a long hydrocarbon chain with a phenyl group attached to every other carbon atom. Expanded Polystyrene (EPS) has strength and stiffness that is comparable to certain types of soils. EPS is about 98% air and just 2% expanded polystyrene. Density is the main structural characteristic of EPS because of its effect on compression strength, shear strength, tension strength, stiffness, and other mechanical properties. The density of EPS ranges from 10 to 30 kg/m³ based on different types of EPS used for different codes. In the experiments conducted for this study, load was applied monotonically; therefore, the corner opening was used just in two ends of the compression diagonal of infill wall. In general, the corner opening must be used in all four corners of an infill wall because of the cyclic loading

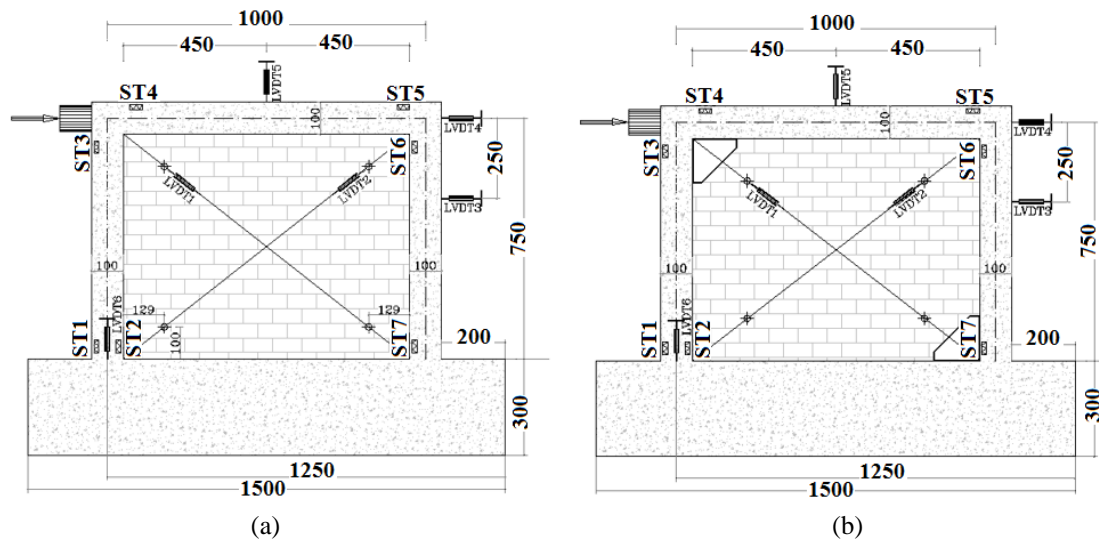


Fig. 8 General layouts of load cell, LVDT and strain gauges of (a) F1(b) F2 specimens

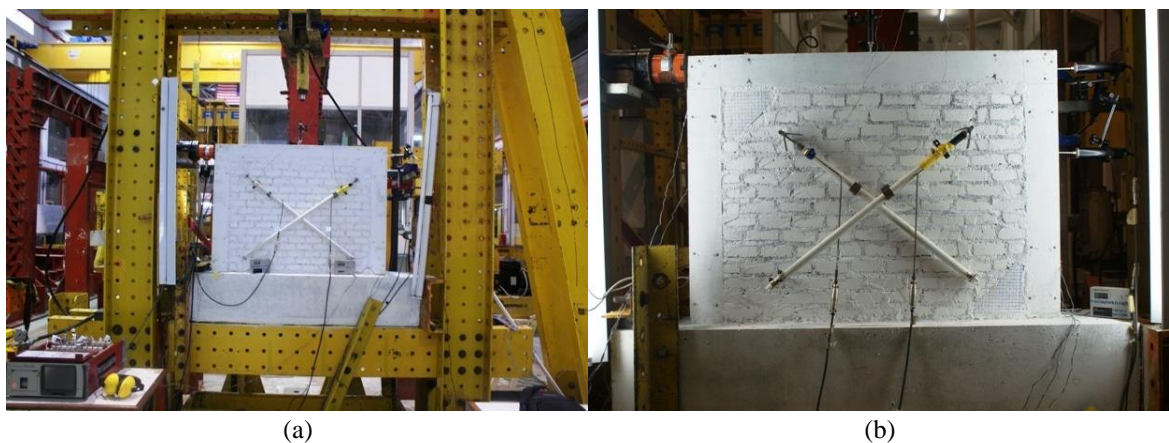


Fig. 9 (a) F1 (b) F2 models setup before the test

caused by earthquakes.

Fig. 9 shows F1 and F2 models before the tests were conducted. In Fig. 9(b), the polystyrene is surrounded by mortar and there is no gap between the materials. To record the response of the specimens, 14 channels were used to log data including 7 strain gauges at different sections of the models and 6 LVTDs. Furthermore, one load cell was used to measure the applied lateral load. Lateral load was applied monotonically to the specimens by a manually control hydraulic system including hydraulic jacks of 300kN and a load cell.

4. Experimental results

To test the diagonal shear strength of walls W1 and W2, loads were applied from zero until the

specimens collapsed. Fig. 10 shows the collapsed state of the specimens. Table 2 shows the results of shear stress, strain, and the shear modulus of the specimens. Shear stress was calculated based on the maximum applied load and the area of the specimens under shear stress as follows

$$\tau = \frac{\text{Cos}(37.87) \times P}{A_n} \quad (8)$$

where, τ is the shear stress on the net area, P is the applied load, $L_v=691$ mm, $L_h=699$ mm, $\alpha=38.87^\circ$, and A_n is net area of the specimen calculated as follows

$$A_n = \left(\frac{W + h}{2}\right)t \quad (9)$$

where, W , H , and t are the width, height, and thickness of specimen in mm. The shear strain is calculated as follows

$$\gamma = \frac{\Delta V + \Delta h}{L_v} \quad (10)$$

where, γ is shearing strain, ΔV is vertical shortening and Δh is the horizontal extension and L_v is the vertical gage length. The modulus of rigidity or modulus of elasticity for shear is calculated as follows

$$G = \frac{\tau}{\gamma} \quad (11)$$



Fig. 10 Collapsed state of (a) W1 and (b) W2 specimens after the diagonal shear strength test

Table 2 Comparison of the results of shear strength test for both specimens

	P_{\max} (kN)	A_n (mm ²) Eq. (9)	τ (MPa) Eq. (8)	γ Eq. (10)	G_{initial} (MPa) Eq. (11)	G (MPa) Eq. (11)	Drift (%) At failure
W1	60.1	40000	1.185	63.67×10^{-5}	1630	1861	0.064%
W2	23.6	40000	0.4655	201.16×10^{-5}	567	231.4	0.2%

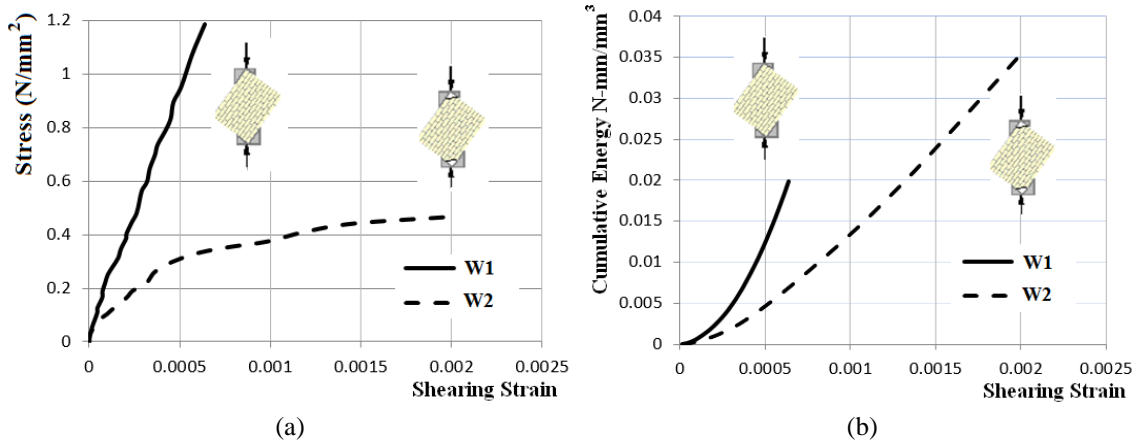


Fig. 11 (a) Stress-strain relation (b) cumulative dissipated energy versus drift for diagonal shear strength tests

4.1 Stiffness and dissipated energy for W1 and W2

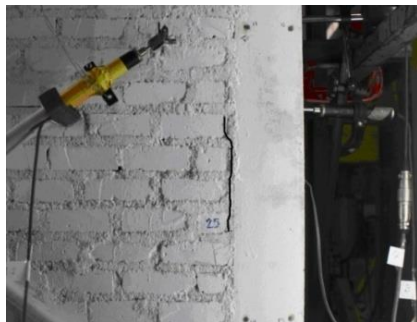
The stress-strain curve for both W1 and W2 are shown in Fig. 11(a). The curve of W1 is almost linear from start to failure indicating brittle behavior but for W2, the curve is nonlinear, which indicates a ductile behavior. The maximum shearing stress was 1.185 and 0.465 MPa for W1 and W2, respectively. The failure strain for W1 and W2 was 63.73E-5 and 201.16E-5, respectively. This means that the maximum shear stress for W1 was about 2.54 times greater than it was for W2 but the failure strain of W2 was 3.15 times greater than it was for W1. Fig. 11(b) shows the cumulative energy stored per unit volume. The cumulative energy stored per unit volume is defined as the sum of the area enclosed by each stress-strain curve. By referring to Fig. 11(b), it is obvious that the W2 has greater capacity (about 1.8 times) to dissipate input energy compare to W1.

4.2 Experimental results for F1 and F2

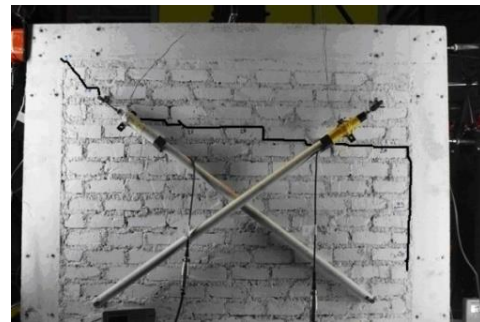
The lateral load was applied to F1 and F2 in three phases at 20% of max strength until the first crack appeared. Lateral load was applied until a drift of 2.5% occurred. A drift of 2.5% is the actual design drift found in the Iranian seismic code (CODE2800). Fig. 12 shows the crack patterns caused by different intensities of lateral loads applied to the specimens. The first separation crack in F1 appeared at a drift of 0.24% and 25 kN of lateral load. The location of crack is in the right edge of the infill and frame boundary (Fig. 12(a)). This is the region labelled O to A in the F1 curve in Fig. 14(a) that shows the linear behavior of the infill wall and frame. At a load of 28 kN (drift 0.29%) this crack horizontally expanded to near the left side of the infill and diagonally continued to left connection of the beam and column (Fig. 12(b)). From 28 kN to 34 kN, the existing cracks widened and extended diagonally into the frame at the left joint. The region labelled A to B of the F1 curve in Fig. 14(a) shows the start of the nonlinear behavior of the system in the formation of cracks in the infill wall. The bars first began to yield at 32 kN (drift 0.37%) for strain gauges ST7. At 35 kN (drift 0.81%) sliding shear cracks formed with a loud sound, as shown in the horizontal region of B to C of the F1 curve in Fig. 14(a). A series of new cracks appeared at

Table 3 The response of specimens to different drift percentages and lateral loads

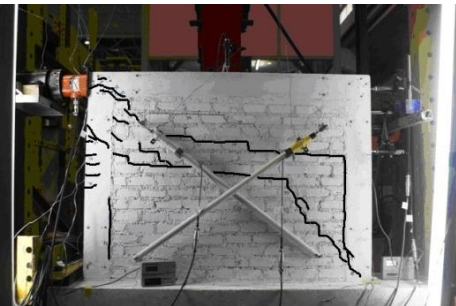
	F1		F2	
	Drift(%)	P(kN)	Drift (%)	P (kN)
First separation	0.24	25	0.12	15
First crack in the infill wall	0.29	28	0.20	17.1
First crack in the Frame	0.29	28	0.24	18.8
Diagonal crack in the infill and frame	-	-	0.37	24.8
First yielding	0.37	32	0.49	30.4
Sliding shear crack in the infill wall	0.81	35	-	-
Propagation of existing cracks	1.0	38	1.0	44.4
Maximum strength	2.5	51.3	1.34	50.9



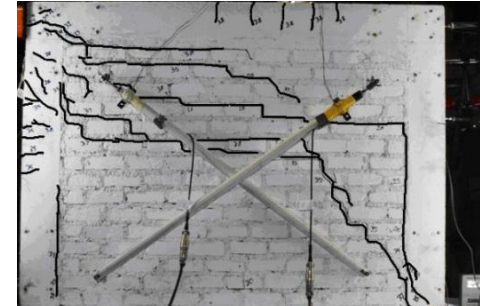
(a) First separation at 25 kN, Drift 0.24%



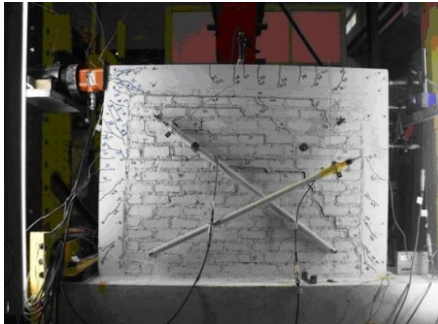
(b) First crack in infill at 28 kN, Drift 0.29%



(c) Sliding shear of infill at 35 kN, Drift 0.81%



(d) Propagation of existing cracks at 38 kN, Drift 1%



(e) Final State of F1 specimen at 51.3 kN, Drift 2.5%



(f) Details of Sliding shear cracks in final state of the test

Fig. 12 Crack patterns at different lateral loads and drifts for F1

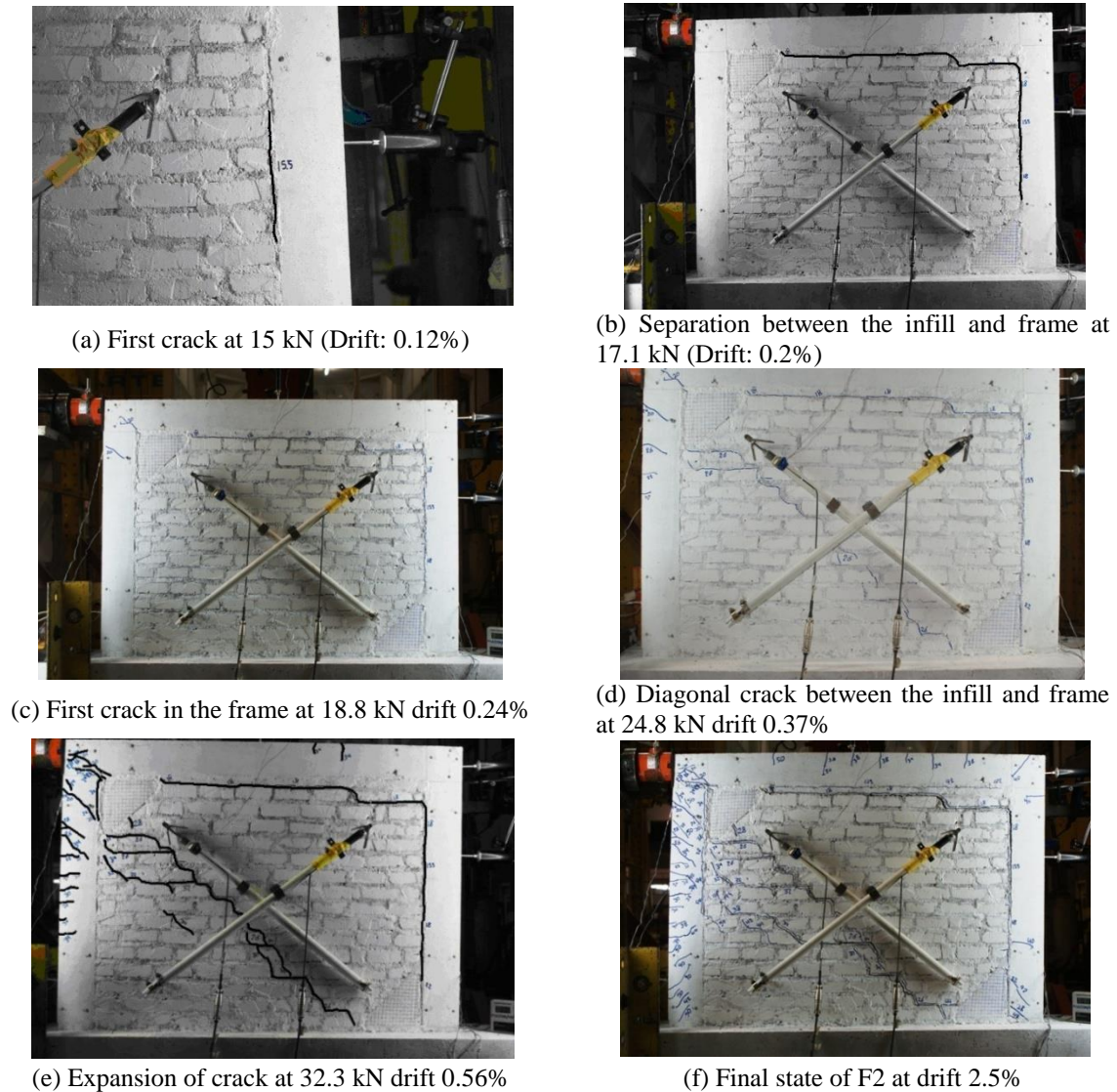


Fig. 13 Crack patterns for different level of lateral load and drift for F2

$0.5H_{col}$ to $0.75H_{col}$ of the left column (H_{col} is height of the columns) (Fig. 12(c)). At this level, a new crack formed between the left side of the infill and the left column at a lower height.

At 38kN (drift 1%), the existing cracks propagated and a series of new cracks appeared in the top part of the beam between $0.5L_{Beam}$ and $0.75L_{Beam}$ (L_{Beam} is the length of the beam) (Fig. 12(d)). At this time, the infill wall completely failed and only the bare frame provided lateral strength until its maximum strength of 51.3 kN (drift 2.5%) (Fig. 12(e)) was reached, which is the region labelled E to F for the F1 curve in Fig. 14(a). Details of sliding shear in the infill wall during the final stages of the experiment are shown in Fig. 12(f). The first separation crack in F2 appeared at drift 0.12% and a lateral load of 15 kN at the same location as the F1 specimen (Fig. 13(a)). This is the region of O to A' of the F2 curve in Fig. 14(a) that shows the linear behavior of the infill wall

and frame. At load 17.1 kN (drift 0.2%) the first separation extended between the infill wall and frame (Fig. 13(b)). The first crack appeared at 18.8 kN (drift 0.24%) in the frame (Fig. 13(c)). A diagonal crack appeared at 24.8 kN (drift 0.37) in the infill wall (Fig. 13(d)). The bars first began to yield at 30.4 kN drift 0.49% for the strain gauges ST1. At load of 32.3 kN and a drift of 0.56%, the cracks expanded on the lower part of the compression diagonal (Fig. 13(e)). Maximum strength of F2 was 50.9 kN at a drift of 1.34% and it gradually decreased until it reached 38.8 kN at a drift of 2.5%. (Fig. 13(f)).

4.3 Stiffness and dissipated energy for F1 and F2

The lateral strength, general behaviour, lateral stiffness, and energy dissipation characteristics results of the specimens were compared. The advantages of the infill frame with a corner opening are discussed. Fig. 14(a) shows the results of lateral load verses a drift curve for F1 and F2. The stiffness of F1 is linear from point *O* to *A*. According to slope of curve the amount of stiffness is about 13.9 kN/mm. The stiffness of F1 gradually reduced from *A* to *B* when the infill separated from the frame. From point *B* to *C*, the infill wall experienced sliding shear failure in infill wall and the stiffness of the system was very low with large horizontal displacement. From point *D* to *E*, the system had an extension in sliding shear with very low stiffness. After point *E*, the stiffness of system comes from the frame. From point *E* to *F*, the stiffness of the system is about 1.26 kN/mm.

Table 4 shows the initial stiffness of the infill wall and frame based on theoretical formulations. The stiffness of F2 is linear from point *O* to *A'* and it is similar to the F1 curve in this region. From point *A'* to *B'* the stiffness of F2 gradually reduced as cracks formed in the infill wall and frame. There were no sliding shear failures or any other significant horizontal displacement. There were some small horizontal areas at 17.1 kN that showed the first signs of separation at 24.8 kN, which was when the first diagonal cracks in the infill wall appeared, and at 38.8 kN, which was the maximum strength of F2. The corner opening in the infill wall prevented major sliding shear failure in the infill wall.

Points *B'* and *F* are the indicators of the systems ultimate strength. It was expected that if two system of F1 and F2 were similar (frame with full infill wall without corner opening) their lateral load capacity and their drift should be the same value. In the current study, the strength of points *B'* and *F* have the same value but their drifts has a different about 1% drift which can be explain by amount of sliding shear drift from point *B* to *E* in F1 model. In fact the amount of horizontal shift between points *B'* and *F* comes from sliding between point *B* and *E* due to sliding shear failure in infill wall in F1 specimen.

Fig. 14(b) shows the cumulative dissipated energy by specimens. The cumulative dissipated energy represents the ability of a structure to absorb the input energy during seismic loads. The cumulative dissipated energy is defined as the sum of the area enclosed by capacity or pushover curve. The curves show that F1 dissipated more energy until drift 1% but that F2 has a greater ability to absorb input energy after drift 1% to drift 2.5%.

Fig. 10 shows both W1 and W2 specimen's failure mode is shear sliding. In these tests, only wall specimens resist against loads. The stress-strain curve in Fig. 11(a) reveals a more ductility behavior and a lower strength of W2 in comparison to W1 specimen. In the tests of frame with walls (F1 and F2), the stiffness of the system is the sum of stiffness of bare frame and infill walls in elastic response region. Moreover, in the test of frame with walls, frame confined the wall. As a result, both of them are interacted and affected on each other's structural response. The strength of

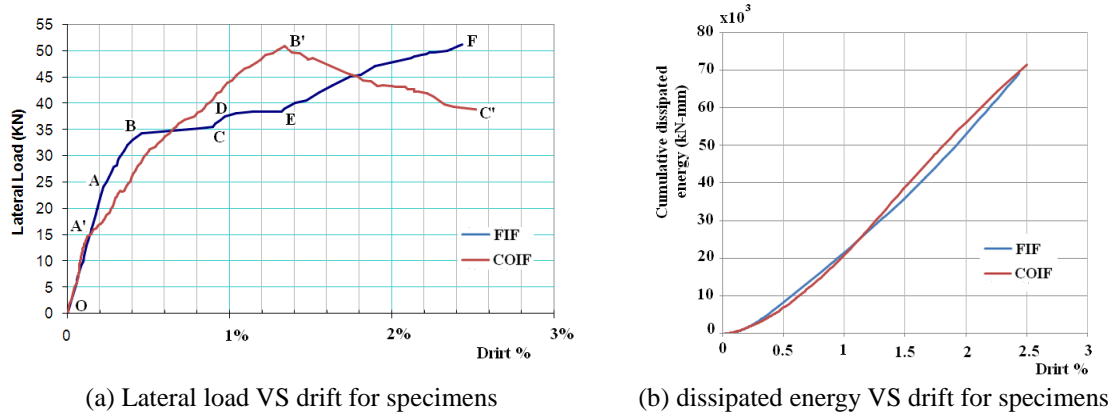


Fig. 14 Crack patterns at different levels of lateral load and drift for F1 and F2

Table 4 Initial stiffness of infill wall and frame system

	E_m^* (MPa)	λ_l	a (mm)	K_{inf} (kN/mm)	K_{frame} (kN/mm)	K_T (kN/mm)
	$E_m = 550f_m$	Eq. (1)	Eq. (2)	Eq. (3)	Eq. (7)	$K_T = K_{inf} + K_{frame}$
F1	3027	0.117	120	10	4.2	14.2

wall with corner opening is less than complete wall and its strength is closer to bare frame strength in comparison to complete wall. On the other hand, the ductility of wall with corner opening is greater than complete wall and its ductility behavior is closer to bare frame. Therefore, in test of frame with corner opening wall (F2), we did not observe a shear sliding and a brittle behavior of infill wall.

5. Conclusions

Infill walls play an important role in the seismic response of a building. The presence of infill walls changes the stiffness, strength, and dynamics parameters of a building. In some cases, infill walls may cause the collapse of buildings when they form a soft story. In this paper a simple method called corner opening, proposed replacing the corner of infill walls with a very flexible material to enhance the structural behavior of infills and the whole structure. To evaluate the proposed method, two infill wall specimens with and without corner opening were constructed and tested under diagonal tension. Additionally, two 1:4 scaled RC frames with infill walls with and without corner opening were constructed and tested under lateral monotonic load until drift 2.5%. The current study was based on scaled specimens, thus using the results for full-scale designs must be carefully considered. The results were presented in terms of lateral load verses drift, and cumulative energy dissipation verses lateral drifts. Based on the results, the following conclusions can be made:

- The corner opening in the infill wall specimen increased the ductility of the infill wall making its seismic behavior similar to that of a ductile RC frame. On the other hand, corner openings will decrease the strength of an infill wall compared to infill wall without corner openings reducing the compression action of the infill wall.
- Infills with corner openings had a nonlinear stress strain curve and its ability to absorb input

energy increased considerably compared to infill walls without corner opening.

- The maximum strength of F1 and F2 was almost the same. In F1, the infill wall failed when subjected to sliding shear before it reached its maximum strength but the corner opening in F2 prevented the major sliding shear failure of the infill wall.
- The first separation between the infill wall and the RC frame occurred at a lower lateral load and drift for F2 specimen than it did for the F1 specimen indicating the behavior of F2 was more nonlinear. On the other hand, in F2, the infill wall participated in a lateral resisting system until the maximum strength of model was reached.
- F2 maintained its integrity in the face of large lateral displacements without sliding failure.

Acknowledgments

The authors would like to thank the staffs of material and structure laboratory of civil engineering department of UTM University.

References

- American Concrete Institute (ACI) (2005), "Building code requirements for structural concrete (Committee 318, ACI 318-05)", American Concrete Institute (ACI), Farmington Hills, MI.
- Asteris, P.G., Antoniou, S.T., Sophianopoulos, D.S. and Chrysostomou, C.Z. (2011), "Mathematical macromodeling of infilled frames: state of the art", *J. Struct. Eng.*, ASCE, **137**(12), 1508-1517.
- ASTM A30 (2011), "Test methods and definitions for mechanical testing of steel products", STM International, 100 Barr Harbor Drive, PO Box C700, West Conshohocken, PA 19428-2959, United State
- ASTM A615 (2011), "Standard specification for deformed and plain billet-steel bars for concrete reinforcement", STM International, 100 Barr Harbor Drive, PO Box C700, West Conshohocken, PA 19428-2959, United State
- ASTM E519/E519M-10 (2011), "Standard Test Method for Diagonal Tension (Shear) in Masonry Assemblages", STM International, 100 Barr Harbor Drive, PO Box C700, West Conshohocken, PA 19428-2959, United State
- ASTM Standards C39/C39M-11a (2011), "Standard Test Method for Compressive Strength of Cylindrical Concrete Specimens", STM International, 100 Barr Harbor Drive, PO Box C700, West Conshohocken, PA 19428-2959, United State
- CODE2800, Building and housing research center (2007), "Iranian Code of practice for seismic resistant design of buildings", Standard No. 2800, 3rd Edition.
- Crisafulli, F.J., Carr, A.J. and Park, R. (2000), "Analytical modeling of infilled frame structures-a general review", *Bull. New Zealand Soc. Earthq. Eng.*, **33**(1), 30-47.
- Dolsek, M. and Fajfar, P. (2001), "Soft storey effects in uniformly infilled reinforced concrete frames", *J. Earthq. Eng.*, **5**, 1-12.
- Egermann, R., Cook, D.A. and Anzani, A. (1991), "An investigation into the behavior of scale model brick walls", *Proceedings of the 9th international brick/block masonry conference*, Berlin.
- FEMA-356 (2000), "Prestandard and Commentary for the Seismic Rehabilitation of Buildings, Federal Emergency Management Agency", Washington, D.C.
- FEMA368 (2000), "NERPH Recommended Provisions for Seismic Regulations for New Building", Seismic Safety Council for the Federal Emergency Management Agency, Washington, D.C
- Hughes, T.G. and Kitching, N. (2000), "Small scale testing of masonry", *Proceedings of the 12th international brick block masonry conference*, Madrid, Spain.
- Kakaletsis, D. (2009), "Analytical modeling of masonry infills with openings", *Struct. Eng. Mech.*, **31**(4),

- 499-520.
- Liauw, T.C. and Kwan, K.H. (1984), "Nonlinear behavior of non-integral infilled frames", *Comput. Struct.* **18**, 551-560.
- Madan, A., Reinhorn, A.M. Mainstone, R.J. (1971), "On the stiffnesses and strengths of infilled frames", *Proc., ICE Suppl.*, **4**, Building Research Station, Garston, UK.
- Murty, C.V.R. and Jain, S.K. (2000), "Beneficial influence of masonry infills on seismic performance of RC frame buildings", *Proceedings, 12th World Conference on Earthquake Engineering*, New Zealand, Paper No. 1790.
- Paulay, T. and Priestley, M.J.N. (1992), *Seismic Design of Reinforced Concrete and Masonry Buildings*, John Wiley & Sons, Inc., New York, NY.
- Polyakov, S.V. (1960), "On the interaction between masonry filler walls and enclosing frame when loaded in the plane of the wall", *Translations in Earthquake Engineering*, EERI, San Francisco.
- Pujol, S. and Fick, D. (2010), "The test of a full-scale three-story RC structure with masonry infill walls", *Eng. Struct.*, **32**, 3112-3121.
- SerkanMisira, I., Ozcelik, O., Girgin S.C. and Kahraman, S. (2012), "Experimental work on seismic behavior of various types of masonry infilled RC frames", *Struct. Eng. Mech.*, **44**(6), 763-774.
- Tasnimi, A.A. and Mohebkhah, A. (2011), "Investigation on the behavior of brick-infilled steel frames with openings, experimental and analytical approaches", *Eng. Struct.*, **33**, 968-980.
- Taunton, P.R. (1997), *Centrifuge 'Modeling of soil/masonry structure interaction'*, Cardiff University, UK.